Bounding the Classical Capacity of Multilevel Damping Quantum Channels

Chiara Macchiavello*
Quit group, Dipartimento di Fisica, Università di Pavia, via A. Bassi 6, I-27100 Pavia, Italy
Istituto Nazionale di Fisica Nucleare, Gruppo IV - Sezione di Pavia, via A. Bassi 6, I-27100 Pavia, Italy and
Istituto Nazionale di Ottica - CNR, Largo E. Fermi 6, I-50125, Firenze, Italy

Massimiliano F. Sacchi†
Istituto di Fotonica e Nanotecnologie - CNR, Piazza Leonardo da Vinci 32, I-20133, Milano, Italy and
Quit group, Dipartimento di Fisica, Università di Pavia, via A. Bassi 6, I-27100 Pavia, Italy

Tito Sacchi‡
Istituto Superiore "Taramelli-Foscolo", via L. Mascheroni 51, I-27100 Pavia, Italy
(Dated: February 8, 2022)

A recent method to certify the classical capacity of quantum communication channels is applied for general damping channels in finite dimension. The method compares the mutual information obtained by coding on the computational and a Fourier basis, which can be obtained by just two local measurement settings and classical optimization. The results for large representative classes of different damping structures are presented.

arXiv:2001.06486v2 [quant-ph] 27 May 2020

I. INTRODUCTION

The complete characterization of quantum communication channels by quantum process tomography [1–3] becomes demanding in terms of state preparation or measurement settings for increasing dimension d of the system Hilbert space since it scales as d^4. Actually, growing interest has been shown recently for quantum communication protocols based on larger alphabets, beyond the binary case with $d = 2$, since they can offer advantages with respect to the two-dimensional case, from higher information capacity to increased resilience to noise [4–7]. Several physical systems allow encoding of higher dimensional quantum information, e.g. Rydberg atoms [8], cold atomic ensembles [9, 10], polar molecules [11], trapped ions [12], NMR systems [13], photon temporal modes [14] and discretized degrees of freedom of photons [15]. Hence, as the size of quantum devices continues to grow, the development of scalable methods to characterise and diagnose noise is becoming an increasingly important problem.

In some situations one is experimentally interested in characterizing only specific features of an unknown quantum channel. Then, less demanding procedures can be adopted with respect to complete process tomography, as for example in the case of detection of entanglement-breaking properties [16, 17] or non-Markovianity [18] of quantum channels, or for detection of lower bounds to the quantum capacity [19–22]. In fact, some properties by themselves are not directly accessible experimentally, as for example the ultimate classical capacity of quantum channels, which generally requires a regularisation procedure over an infinite number of channel uses [23–26]. Moreover, by adopting quantum process tomography to reconstruct just a single use of the channel, we notice that the evaluation of the classical capacity remains a theoretically hard task, even numerically [27–32].

It is therefore very useful to develop efficient means to establish whether a communication channel can be profitably employed for information transmission when the kind of noise affecting the channel is not known. For the purpose of detecting lower bounds to the classical capacity a versatile and proficient procedure has been recently presented in Ref. [33]. The method allows to experimentally detect useful lower bounds to the classical capacity by means of few local measurements, even for high-dimensional systems. The core of the procedure is to efficiently measure a number of probability transition matrices for suitable input states and matched output projective measurements, and then to evaluate the pertaining mutual information for each measurement setting. This is achieved by finding theoretically or numerically the optimal prior distribution for each single-letter encoding. Hence, a lower bound to the Holevo capacity and then a certification of minimum reliable transmission capacity is achieved.

In this paper we apply the above method to detect lower bounds to the classical capacity of general damping channels in dimension $d > 2$. The form of channels we consider has been previously investigated in the context of quantum error correcting codes [34, 35]. We will compare the mutual information achieved by coding on the computational and a Fourier basis, which can be obtained by just two local measurement settings and classical optimization. We present the results for large representative classes of different damping structures for high-dimensional quantum systems.

* chiara.macchiavello@unipv.it
† msacchi@unipv.it
‡ tito.sakki@gmail.com

II. THE GENERAL METHOD

We briefly review the method proposed in Ref. [33]. The classical capacity C of a noisy quantum channel $\mathcal{E}$ quantifies the maximum number of bits per channel use that can be reliably transmitted. It is defined [24–26] by the regularized expression $C = \lim_{n\to\infty} \chi(\mathcal{E}^{\otimes n})/n$, in terms of the Holevo capacity

$$\chi(\Phi) = \max_{\{p_i,\rho_i\}} \{S[\Phi(\textstyle\sum_i p_i\rho_i)] - \textstyle\sum_i p_i S[\Phi(\rho_i)]\} \ , \quad (1)$$

where the maximum is computed over all possible ensembles of quantum states, and $S(\rho) = -\operatorname{Tr}[\rho\log\rho]$ denotes the von Neumann entropy (we use logarithm to base 2). The Holevo capacity $\chi(\mathcal{E}) \equiv C_1$ is a lower bound for the channel capacity, and corresponds to the maximum information when only product states are sent through the uses of the channel, whereas joint (entangled) measurements are allowed at the output. Then, clearly, the Holevo capacity is also an upper bound for any expression of the mutual information [36–38]

$$I(X;Y) = \sum_{x,y} p_x p(y|x) \log \frac{p(y|x)}{\sum_{x'} p_{x'} p(y|x')} \ , \quad (2)$$

where the transition matrix $p(y|x)$ corresponds to the conditional probability for outcome y in an arbitrary measurement at the output for a single use of the channel with input ρ_x, and p_x denotes an arbitrary prior probability, which describes the distribution of the encoded alphabet on the quantum states $\{\rho_x\}$.

In order to detect a lower bound to the classical capacity when the number of measurement settings is smaller than the one needed for complete process tomography, the following strategy can be adopted. Prepare a bipartite maximally entangled state $|\phi^+\rangle = \frac{1}{\sqrt{d}} \sum_{k=0}^{d-1} |k\rangle|k\rangle$ of a system and an ancilla A with the same dimension d; send $|\phi^+\rangle$ through the unknown channel $\mathcal{E}\otimes\mathcal{I}_A$, where $\mathcal{E}$ acts on the system alone; finally, measure locally a number of observables of the form $X_i \otimes X_i^\tau$, where τ denotes the transposition w.r.t. to the fixed basis defined by $|\phi^+\rangle$.

By denoting the d eigenvectors of X_i as $\{|\phi_n^{(i)}\rangle\}$ and using the identity [39]

$$\operatorname{Tr}[(A\otimes B^\tau)(\mathcal{E}\otimes\mathcal{I}_R)|\phi^+\rangle\langle\phi^+|] = \frac{1}{d}\operatorname{Tr}[A\mathcal{E}(B)] \ , \quad (3)$$

the measurement protocol allows to reconstruct the set of conditional probabilities $p^{(i)}(m|n) = \langle\phi_m^{(i)}|\mathcal{E}(|\phi_n^{(i)}\rangle\langle\phi_n^{(i)}|)|\phi_m^{(i)}\rangle$. We can then write the optimal mutual information for the encoding-decoding scheme by the observable X_i as

$$I^{(i)} = \max_{\{p_n^{(i)}\}} \sum_{n,m} p_n^{(i)} p^{(i)}(m|n) \log \frac{p^{(i)}(m|n)}{\sum_l p_l^{(i)} p^{(i)}(m|l)} \ . \quad (4)$$

Then, the following chain of inequalities holds

$$C \geq C_1 \geq C_{DET} \equiv \max_i \{I^{(i)}\} \ , \quad (5)$$

where C_{DET} is the experimentally accessible bound to the classical capacity, which depends on the chosen set of measured observables labeled by i.

Notice that such a detection method based on the measurements of the local operators does not necessarily require the use of an entangled bipartite state at the input. Actually, each conditional probability $p^{(i)}(m|n)$ can be equivalently obtained by testing only the system, i.e. preparing it in each of the eigenstates of X_i, and measuring X_i at the output of the channel.

The maximisation over the set of prior probabilities $\{p_n^{(i)}\}$ in Eq. (4) for each i can be achieved by means of the Blahut-Arimoto recursive algorithm [40–42], given by

$$g_n^{(i)}[r] = \exp\left(\sum_m p^{(i)}(m|n) \log \frac{p^{(i)}(m|n)}{\sum_l p_l^{(i)}[r] p^{(i)}(m|l)}\right) ;$$
$$p_n^{(i)}[r+1] = p_n^{(i)}[r] \frac{g_n^{(i)}[r]}{\sum_l p_l^{(i)}[r] g_l^{(i)}[r]} \ . \quad (6)$$

Starting from an arbitrary prior probability distribution $\{p_n^{(i)}[0]\}$, this guarantees convergence to an optimal prior $\{\bar{p}_n^{(i)}\}$, thus providing the value of $I^{(i)}$ for each i with the desired accuracy. A minor modification of the recursive algorithm (6) can also accommodate possible constraints, e.g. the allowed maximum energy in lossy bosonic channels [43].

We remind that for some special forms of transition matrices $p^{(i)}(m|n)$ there is no need for numerical maximisation, since the optimal prior is theoretically known. This is the case of a conditional probability $p^{(i)}(m|n)$ corresponding to a symmetric channel [44], where every column $p^{(i)}(\cdot|n)$ [and row $p^{(i)}(m|\cdot)$] is a permutation of each other. In fact, in such a case the optimal prior is the uniform $\bar{p}_n^{(i)} = 1/d$, and the pertaining mutual information is given by $I^{(i)} = \log d - H[p^{(i)}(\cdot|n)]$, where $H(\{x_j\}) = -\sum_j x_j \log x_j$ denotes the Shannon entropy and therefore $H[p^{(i)}(\cdot|n)]$ is the Shannon entropy of an arbitrary column (since all columns have the same entropy).

III. MULTILEVEL DAMPING CHANNELS

We apply the general method summarized in the previous Section to quantum channels of the Kraus form

$$\mathcal{E}(\rho) = \sum_{k=0}^{d-1} A_k \rho A_k^\dagger \ , \quad (7)$$

with

$$A_k = \sum_{r=k}^{d-1} c_{r-k,r} |r-k\rangle\langle r| \ . \quad (8)$$

The trace preserving condition $\sum_{k=0}^{d-1} A_k^\dagger A_k = I$ corresponds to the following constraints

$$\sum_{k=0}^{r} |c_{r-k,r}|^2 = 1 \qquad \text{for all } r\,. \tag{9}$$

The above channels represent a generalization of damping channels for d-dimensional quantum systems, where each level can populate only its lower-lying levels, and no reverse transition can occur. This form of channel can thus accommodate different decay processes, from multilevel atoms to dissipative bosonic systems (see for example [45, 46]). The customary amplitude damping channel for qubits is recovered for $d = 2$ and $c_{0,0} = 1$, $c_{0,1} = \sqrt{\gamma}$ and $c_{1,1} = \sqrt{1-\gamma}$.

Typically, for a fixed value of r each column vector $c_{r-k,r}$ will depend on a set of damping parameters such that in a suitable limit for all values of r one has $c_{r-k,r} = \delta_{k,0}$ (or $c_{r-k,r} = \delta_{k,0} e^{i\psi_r}$). In this way, for such a limit one obtains the noiseless identity map $\mathcal{E}(\rho) = \rho$ (or noiseless unitary map $\mathcal{E}(\rho) = U\rho U^\dagger$ where $U = \sum_{r=0}^{d-1} e^{i\psi_r} |r\rangle\langle r|$) [47]. Notice also that if the number of allowed jumps in the level structure is limited to S, one will always have $c_{r-k,r} = 0$ for $k > S$.

We consider the simplest case where only two projective measurements are used to bound the classical capacity, namely the two mutually unbiased bases

$$B = \{|n\rangle,\ n \in [0, d-1]\}\ , \tag{10}$$

$$\tilde{B} = \left\{ |\tilde{n}\rangle = \frac{1}{\sqrt{d}} (\textstyle\sum_{j=0}^{d-1} \omega^{nj} |j\rangle),\ n \in [0, d-1] \right\}\ , \tag{11}$$

with $\omega = e^{2\pi i/d}$. The corresponding transition matrices for "direct coding" (with basis B) and "Fourier coding" (with basis $\tilde{B}$) are given by

$$Q(m|n) = \langle m|\mathcal{E}(|n\rangle\langle n|)|m\rangle\,, \tag{12}$$

$$\tilde{Q}(m|n) = \langle \tilde{m}|\mathcal{E}(|\tilde{n}\rangle\langle \tilde{n}|)|\tilde{m}\rangle\,, \tag{13}$$

respectively. As we have seen, each of these transition matrices can be experimentally reconstructed by preparing a bipartite maximally entangled state and performing two separable measurements at the output of the channel (which acts just on one of the two systems), or equivalently by testing separately the ensemble of basis states with the respective measurement at the output. The detected lower bound C_{DET} to the classical capacity of the channel then corresponds to the larger value between $I^{(B)}$ and $I^{(\tilde{B})}$, which are obtained by Eq. (4).

The present study is inspired by a specific case of damping channel for qutrits studied in Ref. [33], where a transition between two different encodings has been observed as a function of the damping parameters. For increasing dimension, the number of parameters characterizing the channel increases and the solution can become quite intricate. We remind that for the customary qubit damping channel no transition occurs, and the Fourier basis always outperforms the computational basis [33].

From Eqs. (7) and (8) one easily obtains the identity

$$\langle m|\mathcal{E}(|n\rangle\langle l|)|s\rangle = c_{m,n} c^*_{s,l} \delta_{l-s,n-m}\ . \tag{14}$$

Then, one has

$$Q(m|n) = |c_{m,n}|^2\ , \tag{15}$$

and

$$\tilde{Q}(m|n) = \frac{1}{d^2} \sum_{l=0}^{d-1} \sum_{s=0}^{l} \sum_{t=0}^{d-1-l+s} c_{s,l} c^*_{t,l-s+t}\, \omega^{(t-s)(m-n)}. \tag{16}$$

Notice that $\tilde{Q}(m|n)$ just depends on $(m-n) \bmod d$ and hence it has the form of a conditional probability pertaining to a symmetric channel. As noticed in the previous Section, in this case the optimal prior distribution achieving the maximisation in Eq. (4) is always the uniform one, and the corresponding mutual information is given by $I^{(\tilde{B})} = \log d - H[\tilde{Q}(\cdot|n)]$.

On the other hand, the optimal prior distribution $\{\bar{p}_n\}$ for the direct-basis coding can be obtained by the algorithm (6). In this case, as a global measure of the non-uniformity of $\{\bar{p}_n\}$ one can consider its Shannon entropy $H(\{\bar{p}_n\})$. Clearly, one has $0 \le H(\{\bar{p}_n\}) \le \log d$.

Notice that for the direct basis, all channels considered here are such that the output states commute with each other. Since the Holevo bound to the accessible information is saturated for sets of commuting states [48], the detected capacity for the direct basis coincides with the Holevo quantity, namely

$$\begin{aligned} I^{(B)} &= \chi_B \equiv S[\mathcal{E}(\textstyle\sum_n \bar{p}_n |n\rangle\langle n|)] - \textstyle\sum_n \bar{p}_n S[\mathcal{E}(|n\rangle\langle n|)] \\ &= H[\textstyle\sum_n \bar{p}_n Q(\cdot|n)] - \textstyle\sum_n \bar{p}_n H[Q(\cdot|n)]\ , \end{aligned} \tag{17}$$

where $\{\bar{p}_n\}$ denotes the optimal prior obtained by the Blahut-Arimoto algorithm. On the other hand, the detected capacity for the Fourier basis $I^{(\tilde{B})}$ will be bounded by the Holevo quantity, namely

$$\begin{aligned} I^{(\tilde{B})} &\le \chi_{\tilde{B}} \equiv S[\mathcal{E}(\textstyle\sum_n \frac{1}{d} |\tilde{n}\rangle\langle \tilde{n}|)] - \textstyle\sum_n \frac{1}{d} S[\mathcal{E}(|\tilde{n}\rangle\langle \tilde{n}|)] \\ &= S\left(\frac{1}{d} \textstyle\sum_n \tilde{\rho}_n\right) - \frac{1}{d} \textstyle\sum_n S(\tilde{\rho}_n)\ , \end{aligned} \tag{18}$$

where

$$\begin{aligned} \tilde{\rho}_n &= \mathcal{E}(|\tilde{n}\rangle\langle \tilde{n}|) \\ &= \frac{1}{d} \sum_{m,s=0}^{d-1} |m\rangle\langle s| \sum_{t=m}^{d-1-s+m} c_{m,t} c^*_{s,s+t-m}\, \omega^{n(m-s)}\ . \end{aligned} \tag{19}$$

Notice that

$$\textstyle\sum_{n=0}^{d-1} \tilde{\rho}_n = \sum_{m=0}^{d-1} |m\rangle\langle m| (\sum_{t=m}^{d-1} |c_{m,t}|^2)\ , \tag{20}$$

and hence the first term in Eq. (18) is just given by

$$S\left(\frac{1}{d} \textstyle\sum_n \tilde{\rho}_n\right) = H(\{w_m\})\ , \tag{21}$$

with

$$w_m = \frac{1}{d} \textstyle\sum_{t=m}^{d-1} |c_{m,t}|^2\ . \tag{22}$$

Clearly, the maximum between the two Holevo quantities (17) and (18) provides a better lower bound than C_{DET} to the ultimate classical capacity, but for an unknown quantum channel their evaluation needs complete process tomography. We will consider the values of χ_B and $\chi_{\tilde{B}}$ in order to compare the results of the proposed method with a theoretical bound, since the damping channels in dimension $d > 2$ are theoretically poorly studied and largely unexplored.

In the following we present numerical results for different multilevel damping channels, which explore many illustrative scenarios. For simplicity, we will fix the matrix elements of $c_{m,n}$ as real. This restriction is always irrelevant as regards the direct basis. For $\arg c_{m,n} = f(n-m)$, this also holds for the Fourier basis.

A. Bosonic dissipation

For a bosonic system with energy dissipation the damping structure is typically governed by Binomial distributions, namely

$$Q(m|n) = \binom{n}{m} \gamma_n^{n-m} (1-\gamma_n)^m \,. \tag{23}$$

In principle, notice that each level can be characterized by its own damping parameter $\gamma_n \in [0,1]$. For this model of noise the classical capacity is known [49] for infinite dimension with mean-energy constraint and $\gamma_n = \gamma$ for all values of n. The mean and variance of these distributions are given by

$$\mu_n = n(1-\gamma_n)\,, \tag{24}$$
$$\sigma_n^2 = n\gamma_n(1-\gamma_n)\,. \tag{25}$$

In Figs. 1-3 we present the results of the optimization for the simplest case of $\gamma_n = \gamma$ for all values of n. We notice that for all values of γ and any dimension d the detected classical capacity C_{DET} depicted in Fig. 1 is achieved by the Fourier encoding $\tilde{B}$. In Fig. 2, for $d = 8$, we also report the best theoretical lower bound given by the Holevo quantity $\chi_{\tilde{B}}$ of Eq. (18) and the looser bound obtained by the direct basis B.
In Fig. 3 we plot the rescaled difference

$$\Delta = \frac{\chi_{\tilde{B}} - C_{DET}}{\log d}\,, \tag{26}$$

in order to compare the detected capacity with the Holevo quantity $\chi_{\tilde{B}}$.

B. Hypergeometric channel

We consider here a damping channel with decay structure characterized by hypergeometric distributions, namely

$$Q(m|n) = \frac{\binom{M}{m}\binom{L-M}{n-m}}{\binom{L}{n}}\,. \tag{27}$$

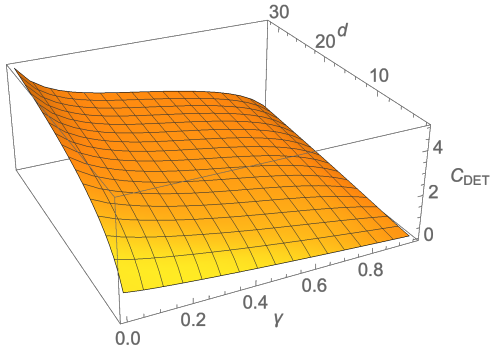


FIG. 1. Detected classical capacity C_{DET} (achieved by the Fourier basis $\tilde{B}$) for a bosonic dissipation channel vs dimension d and damping parameters $\gamma_n = \gamma$.

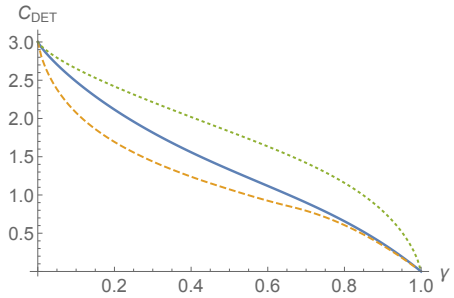


FIG. 2. Detected classical capacity C_{DET} for a bosonic dissipative channel vs damping parameters $\gamma_n = \gamma$ for $d = 8$ (solid line, achieved by the Fourier basis $\tilde{B}$). The looser bound in dashed line corresponds to the direct basis B. The dotted line represents the theoretical lower bound given by the Holevo quantity $\chi_{\tilde{B}}$ of Eq. (18).

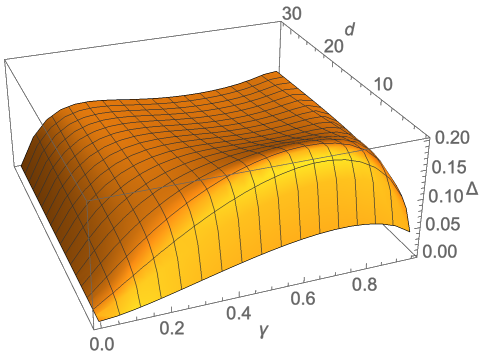


FIG. 3. Rescaled difference Δ between the theoretical Holevo quantity $\chi_{\tilde{B}}$ and the detected classical capacity C_{DET} for a bosonic dissipation channel vs dimension d and damping parameters $\gamma_n = \gamma$.

with integer M and L, with $0 \le M \le L$ (in principle, both M and L could vary for different values of n). This distribution is related to the probability of m successes in n draws without replacement from finite samples of L elements, differently from the binomial distribution where each draw is followed by a replacement. The correspondence with the customary binomial distribution is ob-

tained for $M/L = 1-\gamma$. In fact, the mean and variance are given by [50]

$$\mu = n\frac{M}{L}\,, \tag{28}$$

$$\sigma^2 = n\frac{M}{L}\left(1-\frac{M}{L}\right)\frac{L-n}{L-1}\,. \tag{29}$$

Notice that the variance is shrunk by the factor $\frac{L-n}{L-1}$ with respect to the binomial distribution. For $M, L \to \infty$ with $M/L = p$ one recovers the binomial distribution. We also observe that the support of the distribution is given by $m \in \{\max(0, n+M-L), \min(n, M)\}$. For $M/L = 1$ the channel is lossless, i.e. $c_{m,n} = \delta_{m,n}$.

In Fig. 4 we report the result of the optimization for $d = 8$ and $L = 12$ vs M. Differently from the case of bosonic dissipation, one can observe a transition from the Fourier basis $\tilde{B}$ to the direct basis B in providing the best detected capacity, for increasing value of the damping parameter (i.e. for decreasing value of M for fixed L).

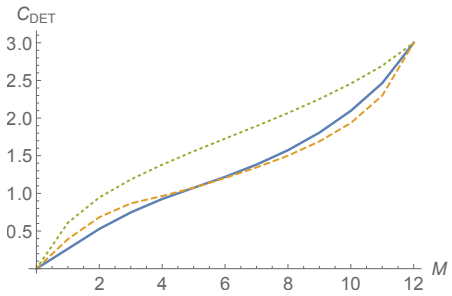


FIG. 4. Detected classical capacity C_{DET} for a damping channel with hypergeometric decay vs parameter M, with $0 \le M \le L = 12$, and dimension $d = 8$. The detected capacity is achieved by the Fourier Basis (solid line) for $M \ge 6$, and by the direct basis B (dashed line) for $M \le 5$. The dotted line represents the theoretical lower bound given by the Holevo quantity $\chi_{\tilde{B}}$ of Eq. (18).

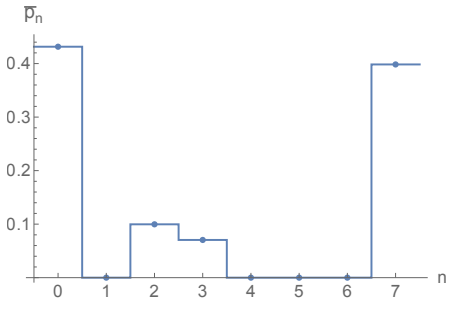


FIG. 5. Optimal prior distribution for the encoding on the direct basis B for a damping channel with hypergeometric decay ($M = 5$ and $L = 12$), in dimension $d = 8$. Among the eight possible input states, just four ($n = 0, 2, 3, 7$) are used for the encoding. The corresponding detected capacity is given by $C_{DET} \simeq 1.074$ bits.

Typically, for increasing values of damping the optimal prior distribution for direct encoding shows holes of zero or negligible probability, as depicted in Fig. 5 for the case $M = 5$ and $L = 12$, with $d = 8$. This can be intuitively understood since in the presence of strong damping it becomes more convenient to use a smaller alphabet of well-spaced letters in order to achieve a better distinguishability at the receiver.

C. Negative hypergeometric channel

We consider now a damping channel with decay structure characterized by negative hypergeometric distributions, namely

$$Q(m|n) = \frac{\binom{m+M-1}{m}\binom{L-M-m}{n-m}}{\binom{L}{n}}\,, \tag{30}$$

with positive integers M and L such that $n \le L - M$ (here also both M and L could vary for different values of n). This distribution is related to the probability of m successes until M failures occur in drawing without replacement from finite samples of L elements. The mean and variance are given by [51]

$$\mu = n\frac{M}{L-n+1}\,, \tag{31}$$

$$\sigma^2 = \mu\left(1-\frac{\mu}{n}\right)\frac{L+1}{L-n+2}\,. \tag{32}$$

Notice that the variance is larger with respect to the binomial distribution. In the limit $M, L \to \infty$ with $M/L = 1-\gamma$ one recovers the binomial distribution.

For this class of channels we generally find that the detected capacity is achieved by the Fourier basis $\tilde{B}$. The results for $d = 8$ and $L = 32$ vs M are reported in Fig. 6.

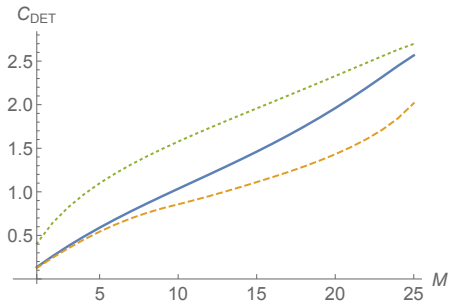


FIG. 6. Detected classical capacity C_{DET} for a damping channel with negative-hypergeometric decay for dimension $d = 8$ and parameter $L = 32$ vs M. The detected capacity is achieved by the Fourier Basis $\tilde{B}$ (solid line), which outperforms the direct basis B (dashed line). The dotted line represents the theoretical lower bound given by the Holevo quantity $\chi_{\tilde{B}}$ of Eq. (18).

D. Beta-binomial channel

We consider a damping channel with decay probabilities given by

$$Q(m|n) = \binom{n}{m} \frac{B(m+\alpha, n-m+\beta)}{B(\alpha,\beta)} , \qquad (33)$$

where $\alpha, \beta > 0$, and $B(\alpha,\beta) = \Gamma(\alpha)\Gamma(\beta)/\Gamma(\alpha+\beta)$ denotes the beta function. This family of distributions arises in binomial trials with success probability that is not known, but distributed according to the beta function. We remind that this distribution can be bimodal (U-shaped), i.e. it can present two peaks when both α and β are smaller than 1. The mean and variance are given by [52]

$$\mu = n\xi , \qquad (34)$$

$$\sigma^2 = n\xi(1-\xi)\frac{\alpha+\beta+n}{\alpha+\beta+1} , \qquad (35)$$

with $\xi = \frac{\alpha}{\alpha+\beta}$. We have then overdispersion with respect to the binomial distribution with $\xi = 1-\gamma$. This binomial is recovered for $\alpha, \beta \to \infty$ with $\xi = 1-\gamma$.

In Figs. 7 and 8 we plot the results of the detected capacity C_{DET} for dimension $d = 8$ as a function of α and β. We notice that C_{DET} is achieved by the Fourier basis $\tilde{B}$ (Fig. 7), except for a tiny region corresponding to very small values of α and β (Fig. 8).
In Fig. 9 we also report the rescaled difference Δ between the Holevo quantity $\chi_{\tilde{B}}$ and C_{DET}.

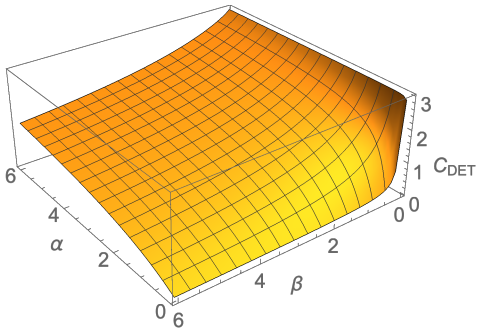


FIG. 7. Detected classical capacity C_{DET} for a beta-binomial decay channel with $d = 8$ vs parameters α and β. In the present region the bound is provided by the Fourier encoding $\tilde{B}$.

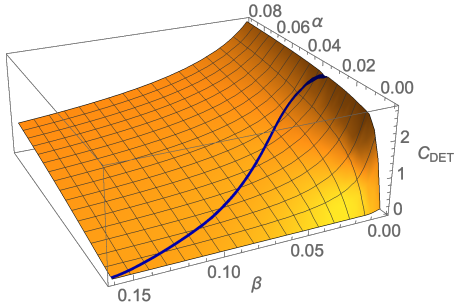


FIG. 8. Detected classical capacity C_{DET} for a beta-binomial decay channel with $d = 8$ vs parameters α and β. In the region below the depicted line the bound is provided by the direct encoding B.

E. Geometric damping

We consider a channel where the decaying conditional probabilities are given by

$$Q(m|n) = \frac{1-\gamma_n}{1-\gamma_n^{n+1}}\gamma_n^{n-m} , \qquad (36)$$

with $\gamma_n \geq 0$.
The results in the simplest case of $\gamma_n = \gamma$ for all values of n are depicted in Fig. 10, where the detected capacity is always achieved by the Fourier basis $\tilde{B}$, for all values of γ and for any dimension d. In Fig. 11 we report the rescaled difference with respect to the Holevo quantity $\chi_{\tilde{B}}$.

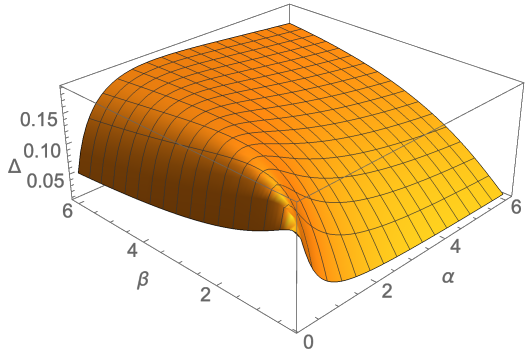


FIG. 9. Rescaled difference Δ between the Holevo quantity $\chi_{\tilde{B}}$ and C_{DET} represented in Fig. 7.

F. Constant ratio for adjacent levels

We consider here a damping channel with constant ratio between the decay probabilities pertaining to adjacent levels, namely we study the case

$$Q(m|n) = \gamma_n^{n-m}(1-\delta_{m,n}) + \frac{1-2\gamma_n+\gamma_n^{n+1}}{1-\gamma_n}\delta_{m,n} , \qquad (37)$$

with suitable positive values for γ_n. The result for $\gamma_n = \gamma$ for all values of n is reported in Fig. 12 for values of the dimension $d = 2, 3, 4$, and 5 [53]. We notice that, except for the qutrit case $d = 3$ with strong decay, the Fourier basis provides a better lower bound to the channel capacity.

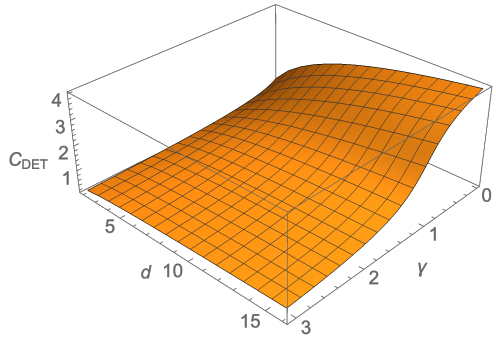


FIG. 10. Detected classical capacity C_{DET} for geometric damping channel vs dimension d and decay parameters $\gamma_n = \gamma$, achieved by the Fourier basis $\tilde{B}$.

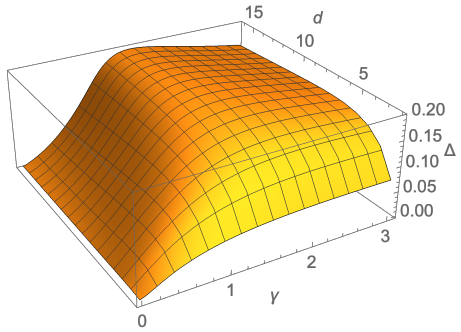


FIG. 11. Rescaled difference Δ between the theoretical Holevo quantity $\chi_{\tilde{B}}$ and the detected classical capacity C_{DET} for a geometric damping channel vs dimension d and damping $\gamma_n = \gamma$.

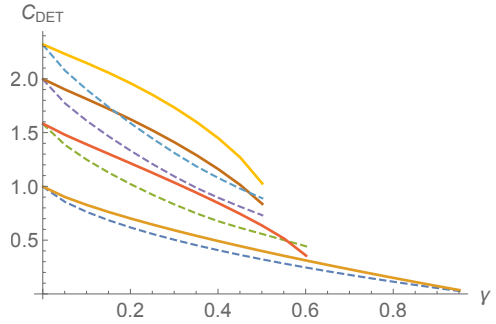


FIG. 12. Detected classical capacity C_{DET} for a constant-ratio decay channel vs allowed values of damping parameter $\gamma_n = \gamma$, for $d = 2, 3, 4, 5$ (from bottom to top). The solid (dashed) lines are referred to the Fourier $\tilde{B}$ (direct B) basis.

G. Two-jump limited damping

The following is an example of a damping channel where each level decays at most by two jumps:

$$Q(0|0) = 1\,,$$
$$Q(m|1) = \frac{1}{1+\gamma_1}(\delta_{m,1} + \gamma_1\delta_{m,0})\,,$$
$$Q(m|n) = \frac{1}{1+\gamma_1+\gamma_2}(\delta_{m,n} + \gamma_1\delta_{m-1,n} + \gamma_2\delta_{m-2,n})$$
$$\text{for } 2 \le n \le d-1\,, \tag{38}$$

with $\gamma_1, \gamma_2 \ge 0$. The results of the detected capacity for dimension $d = 8$ are reported in Fig. 13. We observe a transition from the Fourier to the direct basis in achieving the optimal detection for sufficiently large values of γ_1 and γ_2.

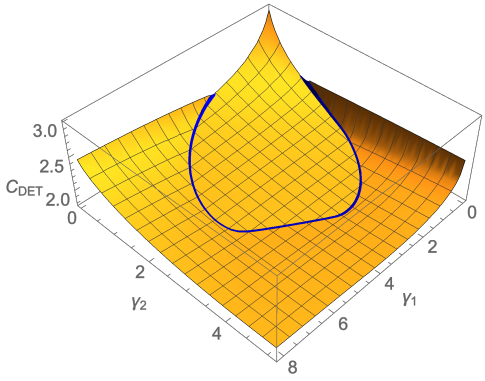


FIG. 13. Detected classical capacity C_{DET} for a two-jump limited decay channel with $d = 8$ vs parameters γ_1 and γ_2. Inside (outside) the enclosed region the bound is achieved by the Fourier basis $\tilde{B}$ (direct basis B).

H. Λ-channels

In this kind of damping channels only the uppermost level interacts with each lower-lying level. Clearly, many variants are possible, and we consider the following case

$$Q(m, d-1) = \frac{1-\gamma}{1-\gamma^d}\gamma^{d-1-m}\,,$$
$$Q(m|n) = \delta_{m,n} \quad \text{for } 0 \le n < d-1\,, \tag{39}$$

with $\gamma \ge 0$. Indeed, this is a particular form of geometric channel, where also the ratio of the transition probabilities pertaining to adjacent levels is constant.

The solution for $d = 4$ is depicted in Fig. 14. We notice that the detected capacity is achieved by the direct basis B, for all values of γ. Interestingly, except for the qubit case $d = 2$ (equivalent to the customary qubit damping channel), we have numerical evidence that the direct basis always provides a better lower bound than the Fourier basis for any γ and d.

I. V-channels

In this last example the lowest level is linked to a succession of higher-lying levels, hence

$$Q(m|n) = (1-\gamma_n)\delta_{n,n} + \gamma_n\delta_{n,0}\,, \tag{40}$$

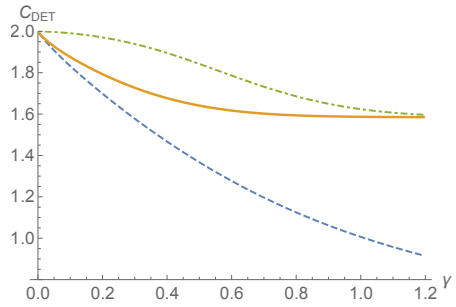


FIG. 14. Detected classical capacity C_{DET} for a Λ-channel vs damping parameter γ for $d = 4$ (solid line, achieved by the direct basis B). The looser bound in dashed line corresponds to the Fourier basis $\tilde{B}$. Since three levels are noise-free $C_{DET} > \log_2 3 \simeq 1.585$ bits. The Shannon entropy of the optimized prior probability $\{\bar{p}_n\}$ is depicted in dot-dashed line.

with $\gamma_n \in [0, 1]$. We considered the simplest case where $\gamma_n = \gamma$ for all values of n, and the detected capacity is plotted in Fig. 15 for values of the dimension $d = 2, 3, 4$, and 8. We notice that for $d = 2$ and 3 the values of the detected capacity of Ref. [33] are recovered. For increasing dimension d we observe a transition: except for the qubit case, where for any γ the best basis is the Fourier $\tilde{B}$, for $d > 2$ the direct basis B rapidly outperforms $\tilde{B}$ for increasing values of γ.

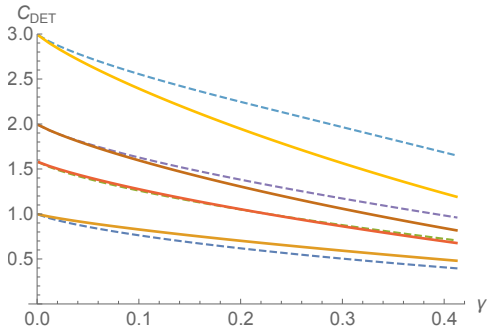


FIG. 15. Detected classical capacity C_{DET} for a V-channel vs damping parameter γ for $d = 2, 3, 4, 8$ (from bottom to top). The solid (dashed) lines are refereed to the Fourier $\tilde{B}$ (direct B) basis.

IV. CONCLUSIONS

We have applied a recently proposed general method [33] to detect lower bounds to the classical capacity of quantum communication channels for general damping channels in dimension $d > 2$. A number of illustrative examples has been considered in the simplest scenario of just two testing measurement settings, namely the direct coding on the computational basis and on a Fourier basis. When the Fourier basis $\tilde{B}$ outperforms the computational basis B, this gives an indication that in such cases the accessible information for a single use of the channel restricted to orthogonal input states and projective output measurements can be improved by coding on non-classical states with respect to the classical coding. As a rule of thumb, we observe that the Fourier basis provides a better lower bound to the classical capacity as long as the variances of the conditional probabilities $Q(m|n)$ pertaining to the direct coding are sufficiently large. The present application to high-dimensional channels strongly supports the use of our method especially when quantum complete process tomography is unavailable or highly demanding, since, as we have shown, remarkable results can be obtained by employing just two measurement settings. In general, by increasing the number of allowed testing measurements, tighter bounds may be obtained. The method we employed is developed for unknown quantum channels. Clearly, when some prior knowledge about the structure of the channel is available, this could be taken into account in the choice of selecting a limited number of suited measurement settings.

ACKNOWLEDGMENTS

C.M. acknowledges support by the European Quantera project QuICHE.

[1] I. L. Chuang and M. A. Nielsen, J. Mod. Optics **44**, 2455 (1997).
[2] M. Mohseni, A. T. Rezakhani, and D. A. Lidar, Phys. Rev. A **77**, 032322 (2008).
[3] I. Bongioanni, L. Sansoni, F. Sciarrino, G. Vallone, and P. Mataloni, Phys. Rev. A **82**, 042307 (2010).
[4] H. Bechmann-Pasquinucci and A. Peres, Phys. Rev. Lett.s **85**, 3313 (2000).
[5] D. Bruss and C. Macchiavello, Phys. Rev. Lett. **88**, 127901 (2002).
[6] N. J. Cerf, M. Bourennane, A. Karlsson, and N. Gisin, Phys. Rev. Lett. **88**, 127902 (2002).
[7] T. Vértesi, S. Pironio, and N. Brunner, Phys. Rev. Lett. **104**, 060401 (2010).
[8] M. Saffman, T. G. Walker, and K. Molmer, Rev. Mod. Phys. **82**, 2313 (2010).
[9] V. Parigi, V. DAmbrosio, C. Arnold, L. Marrucci, F. Sciarrino, and J. Laurat, Nat. Comm. **6**, 7706 (2015).
[10] D.-S. Ding, W.Zhang, S. Shi, Z.- Y. Zhou, Y. Li, B.-S. Shi, and G.-C. Guo, Light: Science & Applications **5**, e16157 (2016).

[11] B. Yan, S. A. Moses, B. Gadway, J. P. Covey, K. R. A. Hazzard, A. M. Rey, D. S. Jin, and J. Ye, Nature **501**, 521 (2013).

[12] C. Senko, P. Richerme, J. Smith, A. Lee, I. Cohen, A. Retzker, and C. Monroe, Phys. Rev. X **5**, 021026 (2015).

[13] I. A. Silva, B. Çakmak, G. Karpat, E. L. G. Vidoto, D. O. Soares-Pinto, E. R. deAzevedo, F. F. Fanchini, and Z. Gedik, Sci. Rep. **5**, 14671 (2015).

[14] B. Brecht, D. V. Ruddy, C. Silberhorn, and M. G. Raymer, Phys. Rev. X **5**, 041017 (2015).

[15] M. Erhard, M. Krenn, and A. Zeilinger, arXiv:1911.10006.

[16] C. Macchiavello and M. Rossi, Phys. Rev. A **88**, 042335 (2013).

[17] A. Orieux, L. Sansoni, M. Persechino, P. Mataloni, M. Rossi, and C. Macchiavello, Phys. Rev. Lett. **111**, 220501 (2013).

[18] D. Chruscinski, C. Macchiavello, and S. Maniscalco, Phys. Rev. Lett. **118**, 080404 (2017).

[19] C. Macchiavello and M. F. Sacchi, Phys. Rev. Lett. **116**, 140501 (2016).

[20] C. Macchiavello and M. F. Sacchi, Phys. Rev. A **94**, 052333 (2016).

[21] A. Cuevas, M. Proietti, M. A. Ciampini, S. Duranti, P. Mataloni, M. F. Sacchi, and C. Macchiavello, Phys. Rev. Lett. **119**, 100502 (2017).

[22] C. Macchiavello and M. F. Sacchi, Phys. Rev. A **97**, 012303 (2018).

[23] M. A. Nielsen and I. L. Chuang, *Quantum Information and Communication* (Cambridge, Cambridge University Press, 2000).

[24] A. S. Holevo, Prob. Inf. Transm. **9**, 177 (1973).

[25] B. Schumacher and M. D. Westmoreland, Phys. Rev. A **56**, 131 (1997).

[26] A. S. Holevo, IEEE. Trans. Inf. Theory **44**, 269 (1998).

[27] S. Beigi and P. W. Shor, http://arxiv.org/abs/0709.2090.

[28] H. Imai, M. Hachimori, M. Hamada, H. Kobayashi, and K. Matsumoto, Proceedings of the 2nd Japanese-Hungarian Symposium on Discrete Mathematics and Its Applications, p. 60 (Budapest, 2001).

[29] S. Osawa and H. Nagaoka, IEICE Trans. on Fundamentals of Electronics, Communications and Computer Sciences **E84**, 2583 (2001).

[30] M. Hayashi, H. Imai, K. Matsumoto, M. B. Ruskai, and T. Shimono, Quantum Inf. Comput. **5**, 13 (2005).

[31] T. Sutter, D. Sutter, P. M. Esfahani, and J. Lygeros, IEEE Trans. Inf. Theory **61**, 1649 (2016).

[32] D. Sutter, T. Sutter, P. M. Esfahani, and R. Renner, IEEE Trans. Inf. Theory **62**, 578 (2016).

[33] C. Macchiavello and M. F. Sacchi, Phys. Rev. Lett. **123**, 090503 (2019).

[34] I. L. Chuang, D. W. Leung, and Y. Yamamoto, Phys. Rev. A **56**, 1114 (1997).

[35] M. Grassl, L. Kong, Z. Wei, Z-Qi Yin, and B. Zeng, IEEE Trans. Inf. Th. **64**, 4674 (2018).

[36] C. A. Fuchs, Phys. Rev. Lett. **79**, 1162 (1997).

[37] A. S. Holevo, Russian Math. Surveys **53**, 1295 (1999).

[38] C. King and M. B. Ruskai, J. Math. Phys. **42**, 87 (2001).

[39] G. M. D'Ariano, P. Lo Presti, and M. F. Sacchi, Phys. Lett. A **272**, 32 (2000).

[40] R. E. Blahut, IEEE Trans. on Inf. Theory **18**, 460 (1972).

[41] R. G. Gallager, *Information Theory and Reliable Communication* (John Wiley & Sons, 1968).

[42] S. Arimoto, IEEE Trans. on Inf. Theory **18**, 14 (1972).

[43] G. M. D'Ariano and M. F. Sacchi, Opt. Commun. **149**, 152 (1998).

[44] T. M. Cover and J. A. Thomas, *Elements of Information Theory*, (Wiley & Sons, New Jersey, 2006).

[45] M. O. Scully and M. S. Zubairy, *Quantum Optics*, (Cambridge University Press, Cambridge, 1997).

[46] R. R. Puri, *Mathematical methods of quantum optics*, (Springer, Berlin, 2001).

[47] A quantum channel corresponds to a discrete state change. Physically, it can be thought of as the integrated solution of an open system dynamics (e.g., a Markovian master equation). Depending on the model, in general the "suitable limit" in the first case corresponds to a small-loss/short-time evolution scenario in the interaction picture. The second case corresponds to the Schroedinger picture, where in the limit only the free Hamiltonian dynamics holds.

[48] D. Petz, Rev. Math. Physics **15**, 79 (2003).

[49] V. Giovannetti, S. Guha, S. Lloyd, L. Maccone, J. H. Shapiro, and H. P. Yuen, Phys. Rev. Lett. **92**, 027902 (2004).

[50] J. A. Rice, *Mathematical statistics and data analysis*, (Belmont, CA Thomson/Brooks/Cole, 2007)

[51] N. L. Johnson, S. Kotz, and A. W. Kemp, *Univariate Discrete Distributions*, (New York, John Wiley & Sons, 1992).

[52] A. K. Gupta and S. Nadarajah, *Handbook of Beta Distribution and its applications*, (Boca Raton, CRC Press, 2004).

[53] The curves cut off in different places for different values of d, because the allowed values of the damping parameter γ depend on the dimension. In fact, Eq. (37) must provide proper normalized conditional probabilities, and this forces different algebraic conditions on γ for different d.